

***Ab initio* study of the LiH phase diagram at extreme pressures and temperatures**Sananda Biswas,^{1,2} Ion Errea,^{3,4} Matteo Calandra,⁵ Francesco Mauri,⁶ and Sandro Scandolo¹¹*The Abdus Salam International Centre for Theoretical Physics, Strada Costiera 11, Trieste, Italy*²*Institut für Theoretische Physik, Goethe-Universität Frankfurt, 60438 Frankfurt am Main, Germany*³*Fisika Aplikatua 1 Saila, Gipuzkoako Ingeniaritza Eskola, University of the Basque Country (UPV/EHU), Europa plaza 1, 20018 Donostia/San Sebastián, Basque Country, Spain*⁴*Donostia International Physics Center, Manuel Lardizabal pasealekua 4, 20018 Donostia/San Sebastián, Basque Country, Spain*⁵*Sorbonne Université, CNRS, Institut des Nanosciences de Paris, UMR 7588, F-75252 Paris, France*⁶*Dipartimento di Fisica, Università di Roma La Sapienza, Piazzale Aldo Moro 5, I-00185 Roma, Italy*

(Received 6 September 2018; revised manuscript received 6 December 2018; published 18 January 2019)

The effect of anharmonic vibrational contributions to the finite-temperature pressure-driven B1-B2 structural phase transition of LiH is studied by using the stochastic self-consistent harmonic approximation method in combination with *ab initio* density functional theory and the quasiharmonic approximation. Contrary to previous experimental results based on multiple-shock compression, we find that the B1-B2 transition pressure is not significantly reduced at high temperatures. Moreover, we find that the B2 phase is dynamically unstable at low temperatures within harmonic theory in a wide range of pressures where its enthalpy is lower than that of the B1 phase, and the inclusion of anharmonic effects stabilizes the B2 phase in this pressure range. Our results imply that a third, yet unknown phase must exist in the phase diagram of LiH, in addition to the B1 and B2 phases, in order to explain the shock compression result.

DOI: [10.1103/PhysRevB.99.024108](https://doi.org/10.1103/PhysRevB.99.024108)**I. INTRODUCTION**

Among the alkali-metal hydrides, LiH has the highest hydrogen mass content and has therefore been widely studied as a potential hydrogen storage material, particularly in the aviation field [1,2]. The recent report of metallization in solid hydrogen at 495 GPa [3] has renewed interest in the high-pressure physics of hydrides. LiH is expected to metallize at lower pressures than hydrogen and is therefore a potential candidate for high-temperature superconductivity [4]. In addition, LiH offers a perfect playground to study the crossover between quantum and classical effects [5]. Its large zero-point energy (ZPE), the quantum vibrational contribution to the energy at zero temperature, suggests that quantum effects play an important role in determining its properties [6,7].

At ambient conditions, LiH crystallizes in the B1 phase, with the NaCl crystal structure, like all other alkali hydrides, and it is a large-gap insulator. Under pressure other alkali hydrides undergo a structural phase transition from B1 to B2 (CsCl structure), with transition pressures decreasing with increasing mass of the alkali atom. The transition pressure varies from 29.3 GPa in NaH to 0.83 GPa in CsH [8,9]. However, in the case of LiH the B2 phase has not yet been found experimentally at room temperature. The B1 phase of LiH was reported to be stable up to a pressure of 252 GPa at 300 K in the diamond-anvil cell experiment of Lazicki *et al.* [10].

First-principles calculations at zero temperature predict a B1-B2 transition at pressures between 313 and 340 GPa, depending on the approximations [11–14]. Theory also predicts that LiH B1 is an insulator up to the transition pressure and becomes a metal upon transforming into B2.

Experimental evidence for a B1-B2 phase transition at high temperature was reported recently by Molodets *et al.* [15] based on multiple-shock compression experiments. They observed the appearance of finite electrical conductivity above 120 GPa and 1800 K and showed, based on a semiempirical theoretical model for the free energy of the two phases, that the experimental finding is consistent with the occurrence of a transition from B1 to B2 at 120 GPa and 1800 K. If this result is compared with the theoretical predictions for the transition pressure at low temperature (313–340 GPa), the conclusion that can be drawn from the experiments of Ref. [15] is that raising the temperature from 300 to 1800 K induces a dramatic decrease of about 200 GPa of the transition pressure.

This strong dependence of the transition pressure of LiH on temperature is surprising and calls for a theoretical analysis. Using the quasiharmonic approximation, Chen *et al.* [16] recently observed that the transition pressure changes only by 50 GPa while increasing the temperature from 0 to 2000 K. These results make us think that the stronger temperature dependence of the transition pressure observed in the multiple-shock compression experiment might arise from hitherto neglected anharmonic contributions to the vibrational free energy, beyond the harmonic or quasiharmonic contributions. So far, the anharmonic contributions in LiH have been studied only in the B1 phase by two research groups: anharmonic effects at ambient condition were investigated by Monserrat *et al.* using a combined vibrational self-consistent field and perturbative approach [17], while Dammak *et al.* studied anharmonic effects as a function of pressure by using quantum thermal bath molecular dynamics and density functional theory (DFT) [18]. Both these studies pointed out that anharmonicity plays an important role in modifying the

vibrational energies of LiH in the B1 phase. However, nothing is known about anharmonicities at high temperature or in the B2 phase.

The goal of this work is to study the role of anharmonicity at finite temperature in B1 and B2 and its impact on the pressure-temperature phase diagram of LiH. We have employed a combination of methods based on *ab initio* DFT, including density-functional perturbation theory (DFPT) [19] in the quasiharmonic approximation and the stochastic self-consistent harmonic approximation (SSCHA) [20]. The rest of the paper is divided into the following sections: we describe the details of our calculations in Sec. II; we describe our results in Sec. III. Finally, we discuss the implications of our results and conclude in Sec. IV.

II. METHOD

All electronic structure calculations were performed using *ab initio* DFT as implemented in the QUANTUM ESPRESSO package [21]. We treated the electron-ion interaction with the projector augmented-wave method [22]. The exchange-correlation functional was approximated by the generalized gradient approximation (GGA) of Perdew, Burke, and Ernzerhof [23]. A plane-wave basis set was used to expand the electronic wave functions. The cutoff for the basis set and the cutoff for the corresponding charge densities were set at 80 and 560 Ry, respectively. Note that both the core and the valence electrons of Li are taken into consideration. The space group of the B1 and B2 phases of LiH are $Fm\bar{3}m$ and $Pm\bar{3}m$, respectively. For both primitive cells Monkhorst-Pack [24] grids of size $20 \times 20 \times 20$ were used to generate the \mathbf{k} mesh (zone centered) for the corresponding Brillouin-zone sampling. The Marzari-Vanderbilt smearing technique [25] was used with a smearing width equal to 0.01 eV for metallic systems.

Electronic structure calculations have been performed on both phases, B1 and B2, at several volumes covering the pressure range of interest. With the above approximations and without inclusion of finite temperature and/or zero-point motion, the calculated lattice constants are 4.00 and 2.51 Å for the B1 and B2 phases, respectively; these values are in good agreement with the previous theoretical (for both B1 and B2) results [13].

In order to obtain the ionic vibrational contributions to the free energy in the harmonic approximation (HA) for both B1 and B2, we have performed calculations based on DFPT [19]. To obtain the harmonic phonon frequencies, the harmonic dynamical matrices were calculated on a $10 \times 10 \times 10$ \mathbf{q} mesh, \mathbf{q} being the wave vector of the corresponding phonon, and the (real-space) interatomic force constant matrices were obtained by inverse Fourier transformation. Using these force constant matrices, the full phonon dispersions for a phase were then obtained by interpolating the dynamical matrices on finer \mathbf{q} -space grids or along high-symmetry lines. It is important to note that the above choices of \mathbf{q} and \mathbf{k} meshes lead to the convergence of zero-point energies E_{ZPE} within 2 meV/LiH. Note that all the values of E_{ZPE} mentioned in Sec. III are calculated within the HA. We would also like to underline the fact that E_{ZPE} can be calculated only for phases which have dynamically stable harmonic phonons.

Anharmonic calculations were performed using either the quasiharmonic approximation (QHA) [26] or the SSCHA [20,27]. In the QHA the anharmonic contribution is obtained from the volume dependence of the harmonic phonons, and its validity is therefore limited to those cases where anharmonicity is small. Note that the application of SSCHA is not restricted to $T \neq 0$ K, and it can also be used to obtain quantum anharmonic effects at $T = 0$ K (as shown in Sec. III C).

It worth mentioning here that one of the greatest advantage of SSCHA is its ability to deal with structures having harmonic phonon instabilities. Another advantage is to deal with strong anharmonicity (when the anharmonic contribution is larger than the corresponding harmonic contribution) by the virtue of being a nonperturbative approach.

For this work, SSCHA calculations were performed by using $3 \times 3 \times 3$ and $2 \times 2 \times 2$ supercells for B1 and B2, respectively. The free energy was initialized by the trial harmonic dynamical matrices obtained using DFPT in the corresponding commensurate \mathbf{q} mesh; for the cases where a harmonic dynamical matrix is not stable at a given \mathbf{q} point, the corresponding trial dynamical matrix has been taken from the regions of volumes where it is stable. The convergence criteria for free energy was set to 1 meV/LiH for one self-consistent (SC) cycle; during such a cycle the number of atomic configurations N_c , obtained by randomly displacing the atoms in the supercell along the modes predicted by the trial/updated dynamical matrices, was kept fixed. Several SC cycles were generally needed in order to have less than 2 cm^{-1} differences in the renormalized phonon frequencies between two consecutive SC cycles. In order to obtain the anharmonic correction, the difference between the harmonic and anharmonic dynamical matrices was then Fourier interpolated to a finer $10 \times 10 \times 10$ \mathbf{q} mesh for both B1 and B2. Finally, adding the harmonic dynamical matrices in the $10 \times 10 \times 10$ \mathbf{q} mesh to this anharmonic correction, the SSCHA dynamical matrices in the finer \mathbf{q} mesh were obtained. All the SC cycles were carried out with $N_c = 20$ configurations, except for the final one, where $N_c = 400$ had been considered.

Note that all the above calculations were performed at fixed volumes of B1 and B2 at different temperatures. The corresponding pressures at these volumes were obtained from the Birch-Murnaghan equation of state (EOS) through the appropriate energies (with or without vibrational contributions, depending on the case) of the respective phases [28].

III. RESULTS

A. Structural stability

At temperature $T = 0$ K, the thermodynamic stability of a phase is determined by the value of the corresponding enthalpy H at a given pressure P , which can be expressed as

$$H(P) = E_{\text{DFT}}(V(P)) + E_{\text{ZPE}}(V(P)) + PV(P), \quad (1)$$

where E_{DFT} and E_{ZPE} are the electronic contributions calculated using DFT and the zero-point vibrational contribution to the energy, respectively, both calculated at the volume V corresponding to pressure P .

Neglecting the zero-point energy, our DFT calculations give a value of 320 GPa for the B1-B2 transition pressure P_{Tr} [12,13]. The B1 phase is insulating at ambient conditions with an experimental band gap of 4.94 eV [29] and has been reported to remain an insulator up to at least 120 GPa [10]. Accurate calculations based on the GGA + GW approximation [12] reproduce very well the band gap at ambient pressure and predict that B1 remains an insulator up to the theoretical transition pressure to B2. According to these calculations, the band gap of B1 decreases with pressure, and it is 0.8 eV at the transition pressure. A similar behavior is predicted by GGA calculations, although the B1 band gap vanishes at the transition pressure within this approximation. On the contrary, local-density approximation calculations erroneously predict a closing of the band gap well within the domain of stability of B1. All previous calculations predict a metallic nature for B2 at and above the transition pressure. Our calculations, based on GGA, give a band gap of 2.98 eV at ambient pressure that vanishes at 320 GPa. Regarding B2, we find that the gap closes at 50 GPa, i.e., much lower than the transition pressure, in agreement with earlier studies by Wang *et al.* [11]. Also, our result is in good agreement with the earlier finding that the B1-B2 transition coincides with the insulator-metal transition in LiH.

In order to determine the ZPE contribution and to check the dynamical stability of the two phases, we performed phonon calculations at different pressures for both B1 and B2. In Fig. 1(a), we show the pressure dependence of the phonon dispersion in B1 along some high-symmetry lines of its Brillouin zone. We find that B1 is dynamically stable throughout the pressure range of interest. At a pressure $P \geq 300$ GPa, there is an incipient softening of the transverse-acoustic (TA) mode at the high-symmetry point **X**; however, the mode never becomes unstable up to the highest pressure considered in this study. We compare our results with previous experimental and theoretical results in Fig. 1(b), where we show the frequencies of all four modes at **X**—TA, longitudinal acoustic (LA), transverse optical (TO), and longitudinal optical (LO)—as a function of (V/V_0) , where V_0 is the volume of the B1 phase at ambient conditions. We find that our results agree well with the previous experimental results (see open circles) [10]. However, our results deviate significantly from the previous theoretical results by Zhang *et al.* [30] when $V/V_0 < 50\%$; in particular, we find that the TA frequency starts to decline at much smaller volumes (i.e., at higher pressures) than in the case of Ref. [30]. Notice that the volume at which Zhang *et al.* find the TA frequency to vanish is within the range of stability of B1, as later determined with x-ray diffraction by Lazicki *et al.* [10], so their results are clearly inconsistent with experiments. We trace the origin of this discrepancy to the use of the frozen-core approximation (FCA) by these previous authors for Li $1s^2$ in the entire pressure range considered by them. Grüneis [14] showed that the FCA holds only around the equilibrium lattice constant of LiH and also showed that FCA underestimates the value of P_{Tr} by 60 GPa.

We now move to the phonon spectra of B2. Yu *et al.* [13] found that LiH B2 is dynamically stable above 160 GPa and displays a phonon instability at point *M* in the Brillouin zone below 160 GPa. In Fig. 2(a), we show our calculated pressure dependence of the phonon dispersions of B2 along

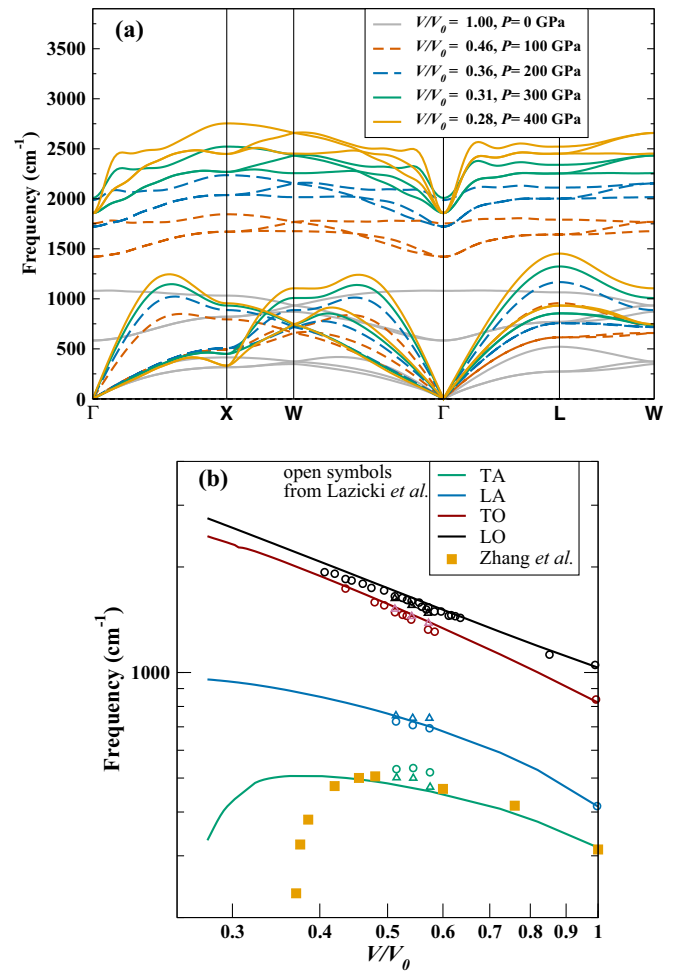


FIG. 1. (a) Phonon dispersion of LiH B1 as a function of pressure along the high-symmetry points of the Brillouin zone. (b) The frequency of the transverse acoustic mode of the B1 phase at **X** as a function of pressure. Our results are represented by lines, and the results from Refs. [10,30] are represented by open symbols and solid orange squares, respectively.

high-symmetry lines of the corresponding Brillouin zone. Unstable phonon modes are represented by negative frequency values throughout this paper. At ambient pressure we find that B2 has a phonon instability over an extended region of the **q** space, including the *M* point. At 100 GPa the instability is confined to a region close to the **X** point, and at about 150 GPa the instability at **X** is also lifted. However, at pressures higher than 150 GPa we continue to observe the presence of an elastic instability at small **q** along the high-symmetry line Γ -**X**. Because phonon dispersions in Fig. 2(a) have been obtained by interpolating frequency calculations on a coarser $10 \times 10 \times 10$ grid than the width in the **q** space of the elastic instability, we checked the accuracy of the frequency determinations close to Γ by performing calculations at **q** points $(1/20, 0, 0)$ and $(1/10, 0, 0)$. For these calculations we used a denser **k**-mesh grid ($40 \times 40 \times 40$). The results are shown in Fig. 2(b) and confirm the results obtained with a coarser **q** mesh. In particular we find that the elastic instability persists up to 420 GPa, above which LiH B2 finally becomes dynamically stable.

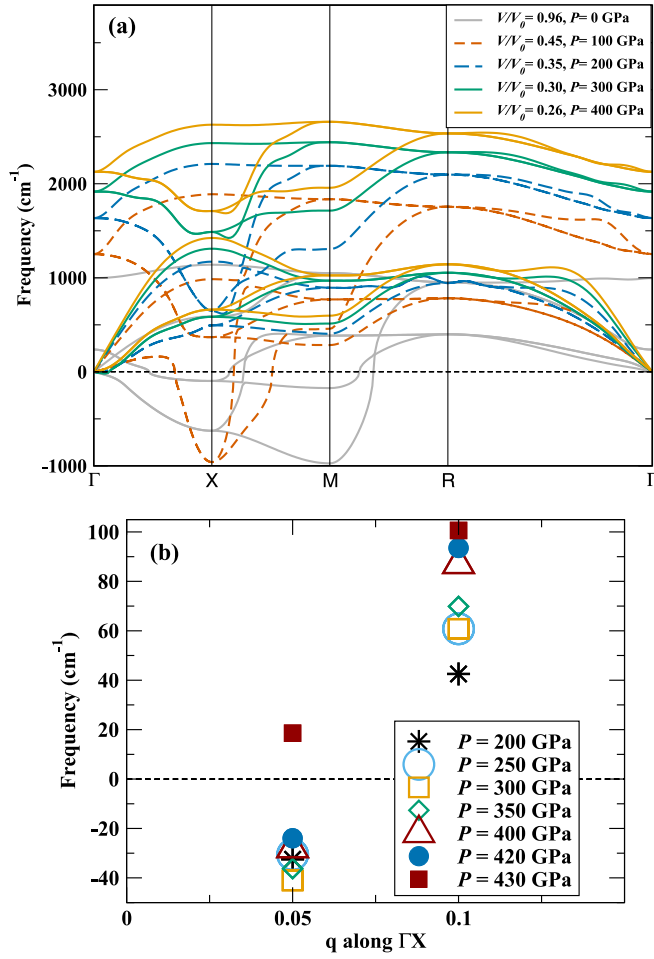


FIG. 2. (a) Phonon dispersion of LiH B2 as a function of pressure along the high-symmetry points of the Brillouin zone. (b) Frequency at two \mathbf{q} points at a denser \mathbf{k} mesh of $40 \times 40 \times 40$ for different values of pressure.

An important consequence of this finding is that a window of pressure exists between the B1-B2 transition pressure 300–350 and 420 GPa, where B2 is dynamically unstable and where therefore either (i) the thermodynamically stable phase of LiH is neither B1 nor B2 or (ii) B2 is stabilized by quantum effects. Before analyzing in more detail the behavior of LiH in this pressure window, let us remark that inclusion of ZPE in Eq. (1) for B1 (at all pressures) and B2 (above 420 GPa) and extrapolation of the B2 enthalpy to $P < 420$ GPa lead to an estimated B1-B2 transition pressure of 318 GPa, in good agreement with previous calculations, with ZPE included [13].

We now concentrate on the pressure window where B2 displays the elastic instability shown in Fig. 2(b). We searched for a lower-enthalpy structure by distorting the B2 structure applying strains corresponding to the unstable phonon branch. We obtained a monoclinic structure with space group $P2_1/m$. We will refer to this structure as distorted B2 (d-B2). In Figs. 3(a)–3(c), we plot the difference in energy δE between B2 and d-B2, as a function of the monoclinic angle α at three different values of pressure ($\alpha = 90^\circ$ corresponds to B2). We find that the value of δE and the amount of deformation

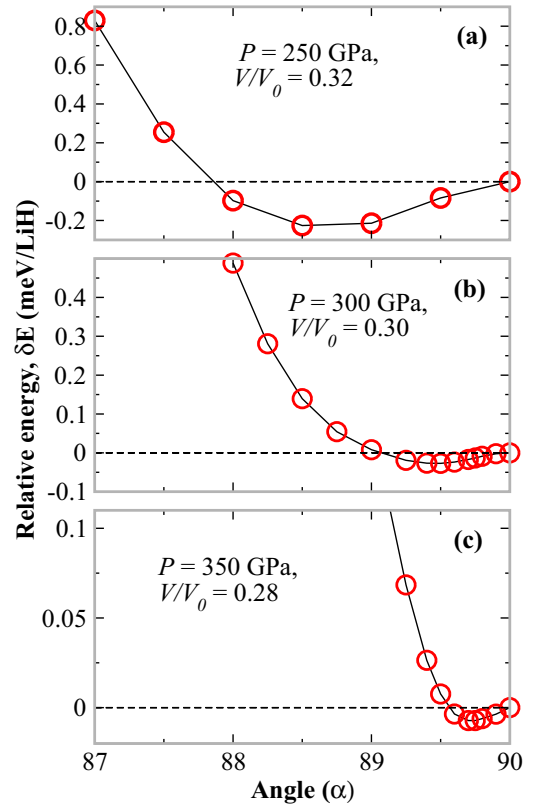


FIG. 3. Relative energy $\delta E = E(\text{d-B2}) - E(\text{B2})$ is plotted as a function of the monoclinic angle at (a) $V/V_0 = 0.32$, (b) $V/V_0 = 0.30$, and (c) $V/V_0 = 0.28$. $\delta E < 0$ indicates that the distorted B2 (d-B2) is more stable than the B2 phase in LiH.

decrease as we increase pressure from 250 to 350 GPa, which is consistent with the disappearance of the instability at 420 GPa inferred from Fig. 2(b).

We also find that the magnitude of the distortion is extremely small. The equilibrium angle deviates by less than a degree from 90° , and the energy gain δE is at least two orders of magnitude smaller than thermal energies at ambient temperature. While it cannot be excluded that d-B2 remains stable at ambient and higher temperatures or after inclusion of quantum effects, anharmonicity is likely to lift the dynamical instability of B2, as it does in other systems [31–33]. In any event, a calculation of the relative free energy between B2 and d-B2 at finite temperature and/or with quantum effects is beyond the scope of this work, so in the remaining part of this work, where we focus on finite-temperature properties, we will perform calculations only for B1 and *undistorted* B2.

B. Phase diagram at finite temperatures

Having discussed the structural stability and the phase diagram at $T = 0$ K and in the harmonic limit, we now move to the investigation of the finite-temperature portion of the phase diagram and to the inclusion of anharmonic contributions. As stated in Sec. II, finite-temperature effects on the crystal free energy can be added in two different ways: (a) by using the quasiharmonic approximation and (b) by using the stochastic self-consistent harmonic approximation.

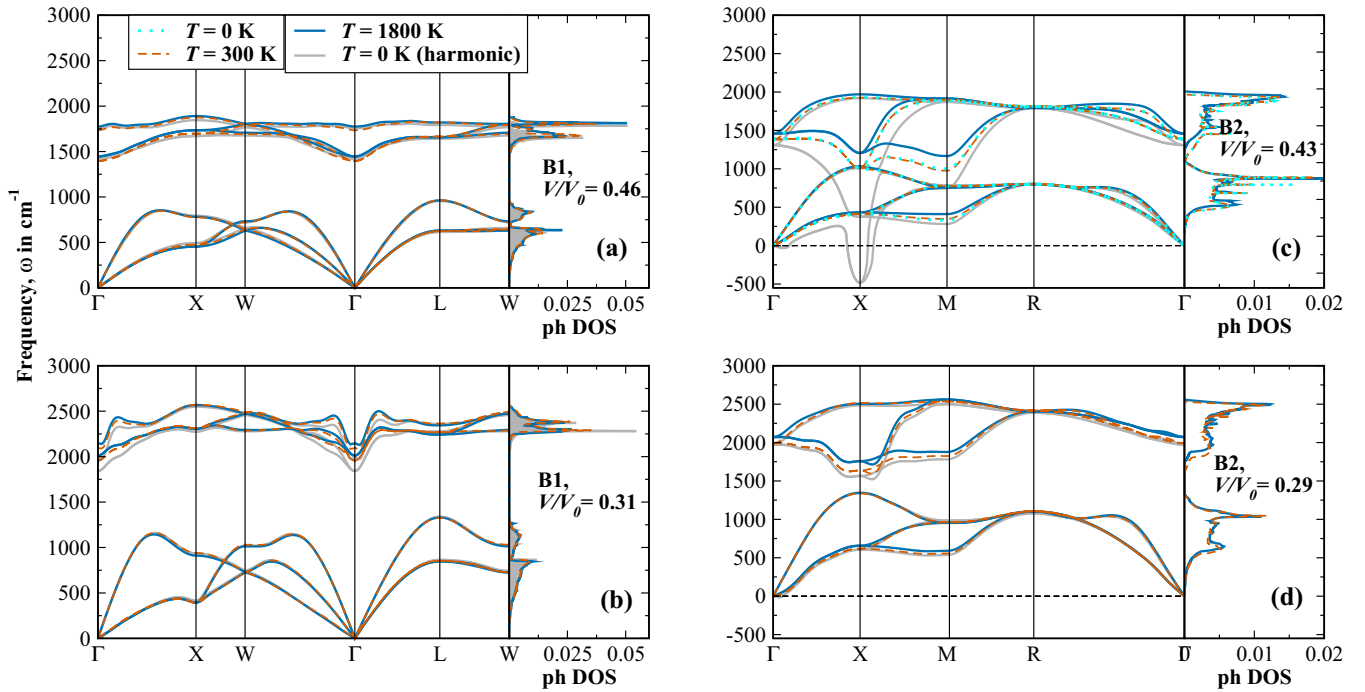


FIG. 4. Comparison of phonon dispersions and the phonon density of states (ph DOS) of (a) and (b) B1 and (c) and (d) B2 at $T = 300$ K (dashed orange line) and $T = 1800$ K (blue line) obtained by SSCHA calculations with the corresponding results obtained at $T = 0$ K (gray line) obtained using HA. Note that the anharmonic effects to phonon dispersions and the phonon DOS at $T = 0$ K are shown by the cyan line in (c). For B2, the phonon DOS has been shown only for stable phonons.

The SSCHA offers at least two advantages over the QHA: (a) it enables one to investigate the role of temperature even when the structure is dynamically unstable within the HA, and (b) it allows the calculation of the anharmonic contributions beyond the perturbative regime, including at $T = 0$ K [20,27]. We therefore begin our analysis of the finite-temperature effects on the LiH phase diagram by analyzing the dynamical stability of B1 and B2 at different temperatures, within the SSCHA. In Fig. 4 we show the phonon dispersions calculated at different temperatures with the SSCHA method, and we compare them with the harmonic dispersions for B1 [Figs. 4(a) and 4(b)] and B2 [Figs. 4(c) and 4(d)].

We find that in both B1 and B2, the phonon frequencies are modified by temperature. Except for B2 at low pressure, we find that the optical phonons harden at high temperature, whereas the acoustic phonons remain almost unchanged. Optical modes have a predominant hydrogen component, contrary to acoustic modes which are dominated by Li. The finding that anharmonicities are stronger for hydrogen-dominated modes is consistent with the lower mass of H. The largest departure with respect to the harmonic limit is found in B2 at low pressure. The prominent harmonic phonon instability at X is removed at all temperatures (from 0 to 1800 K) by the anharmonic contribution. The stabilization of the B2 structure already at $T = 0$ K indicates that quantum effects are crucial for the structural stability of B2. Increasing temperature from 0 to 1800 K increases the stability of the B2 structure, although by a smaller extent with respect to the contribution of quantum effects at 0 K. We verified that the calculation of the phonon spectra from the SSCHA free-energy Hessian [34] keeps the system dynamically stable at the X point. The

correction imposed by the latter calculation to the auxiliary SSCHA phonons plotted in Fig. 4 is just a slight redshift.

In order to clearly show that anharmonic effects remove the harmonic phonon instabilities of the B2 phase in the entire pressure range of this study, especially in the pressure range where B2 wins over B1 in terms of enthalpy (see Sec. III A), we have plotted the phonon dispersions at $T = 300$ K for various volume fractions (corresponding to the pressure range of harmonic phonon instabilities) in Fig. 5(a). Figure 5(b) shows a zoomed-in region of the phonon dispersion along the

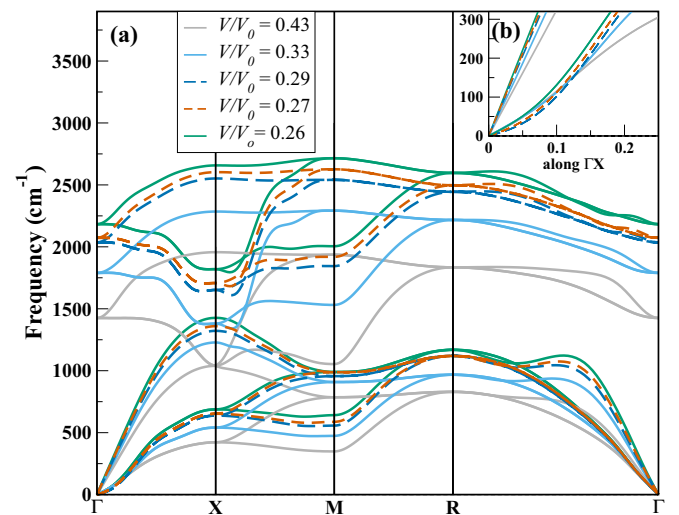


FIG. 5. (a) Phonon dispersions of LiH B2 as a function of volume fractions at $T = 300$ K. (b) A zoomed-in region of (a) along Γ -X.

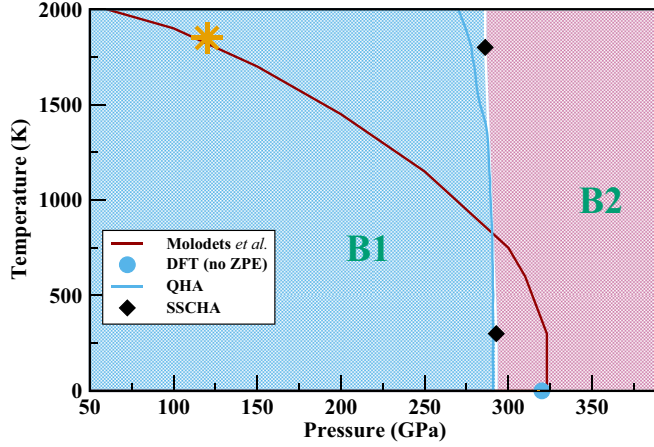


FIG. 6. B1-B2 phase diagram. Blue and pink regions represent the regions of phase stability of B1 and B2, respectively, obtained from SSCHA. The blue line represents the transition line obtained from QHA. The red line represents the transition line suggested by Ref. [15]; the orange star represents the position of the appearance of electrical conductivity observed by these authors.

Γ -X direction where phonon frequencies become positive due to the inclusion of anharmonic effects. A similar behavior is observed at $T = 1800$ K.

In order to determine the relative stability of B1 versus B2, we calculate the Gibbs free energy of the two phases:

$$G(P, T) = F(V(P, T), T) + PV(P, T), \quad (2)$$

where $V(P, T)$ is obtained by inverting $P = -(\partial G / \partial V)_T$. The Helmholtz free energy is approximated by

$$F(V, T) = E_{\text{DFT}}(V, T = 0) + F_{\text{vib}}(V, T), \quad (3)$$

where $F_{\text{vib}}(V, T)$ is the total vibrational contribution to F (including the ZPE), calculated in the QHA or in the SSCHA. At the temperatures of interest for this work the temperature dependence of the electronic energy is negligible [16].

As the QHA can be employed only for dynamically stable phases, a QHA-based determination of F_{vib} would have to be limited to the pressure range $P > 420$ GPa, where B2 is dynamically stable. However, as discussed at the end of the previous section, the dynamical instability of B2 observed above 150 GPa leads to an enthalpy gain that is at least two orders of magnitude smaller than thermal energies. In the remaining part of this study we will assume that temperature removes the instability, and we will technically compute QHA averages over the phonon Brillouin zone (BZ) by setting frequencies to zero in the tiny portion of the B2 BZ (about 10^{-4} of the whole BZ) where they are imaginary. The B1-B2 transition pressure thus obtained is shown as a blue line in Fig. 6. Note that the calculated values of the transition pressure P_{Tr} are 291 and 278 GPa at $T = 300$ and 1800 K, respectively. It is worth mentioning that due to the differences in the methods used, the $T = 0$ K behavior of the QHA transition line does not exactly correspond to the zero-point energy corrected transition pressure at $T = 0$ K (see Sec. III A).

With the SSCHA approximation, we find that the values of P_{Tr} for the B1-B2 transition are 293 GPa at 300 K and

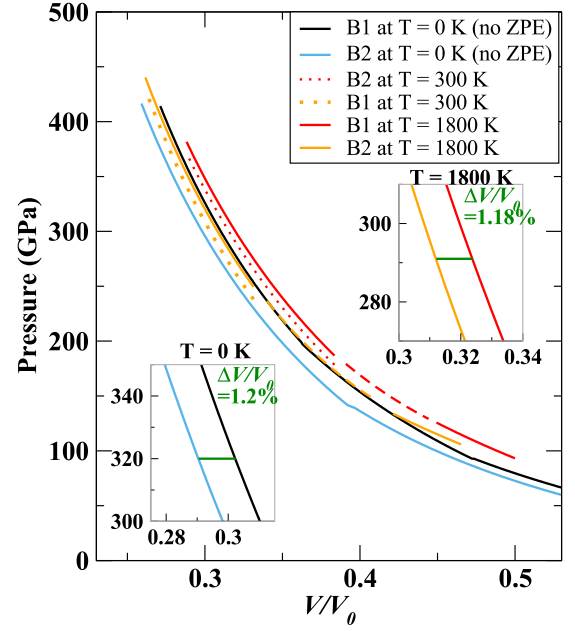


FIG. 7. Equation of states (EOS) at $T = 0, 300$, and 1800 K. The solid black and blue lines represent the EOSs of B1 and B2, respectively, at $T = 0$ K; the solid (dotted) orange and red lines represent the EOSs of B1 and B2, respectively, at $T = 1800$ K (300 K). The insets show the percentage of change of volume $\Delta V / V_0$ at the corresponding transition pressures at a given temperature (shown by green horizontal lines).

286 GPa at 1800 K. These values are considerably smaller than the transition pressure calculated at $T = 0$ K without vibrational contributions (320 GPa). Therefore quantum effects are essential for a quantitative determination of the transition pressure. Moreover, the difference between the results obtained with the QHA and SSCHA approximations indicates that anharmonic effects cannot be neglected. The phase diagram at finite temperatures was obtained by interpolating SSCHA calculations of the B1-B2 transition pressure at two different temperatures ($T = 300$ and 1800 K) and is shown in Fig. 6. Differences between the QHA and SSCHA grow with temperature, indicating that anharmonic effects become more relevant as temperature is increased, as expected. Within both approximations the transition line bends towards lower pressures when temperature is increased, indicating that the vibrational entropy of B2 is higher than that of B1. We have taken the value of P_{Tr} at $T = 0$ K to be the same as that at $T = 300$ K obtained by SSCHA calculations. In Fig. 7 we show the equation of states for B1 and B2 at $T = 0, 300$, and 1800 K. We find that the effect of temperature on the EOSs of B1 and B2 is similar. The volume jump at the transition pressure is slightly smaller (1%) at $T = 1800$ K than at $T = 0$ K (1.2%).

IV. DISCUSSION AND CONCLUSIONS

Our calculated phase diagram indicates that the B1-B2 transition pressure of LiH does not reduce significantly with increasing temperatures, contrary to the prediction made by Molodets *et al.* [15] based on shock-wave experiments. The

B1-B2 transition line proposed by Molodets *et al.* would have implied a reduction of more than 200 GPa in the B1-B2 transition pressure upon increasing temperature from ambient to 1800 K (see red line in Fig. 6), much larger than our calculated value. The onset of conductivity observed in shock-wave experiments at 120 GPa and 1800 K must therefore originate from a different type of transition. We checked if metallization within the B1 phase could provide an explanation for the shock-wave results, without invoking the presence of a structural phase transition. To this aim, we computed the electronic structure of all the converged atomic configurations ($N_c = 200$) for B1 at $T = 1800$ K at 120 GPa and found that all of them have a finite band gap of at least 0.9 eV. We can therefore rule out metallization in

B1 as a reason for the shock-wave discontinuity. Incidentally, we notice that Monserrat *et al.* [17] also found a positive slope for the temperature dependence of the B1 band gap at ambient pressure.

We conclude that the onset of conductivity seen in the shock-wave experiment of Molodets *et al.* [15] must originate from a structural phase transition to a so far unknown phase. In addition, we find that the anharmonic vibrational contributions remove harmonic phonon instabilities of the B2 phase, especially in the region of pressure where B2 wins over B1 in terms of enthalpy. Further work is required to shed light on the open questions which imply the presence of one or maybe more yet to be determined phases of LiH in the megabar regime.

-
- [1] R. van Houten, *Nucl. Eng. Des.* **31**, 434 (1974).
 - [2] V. Tyutyunnik, *Phys. Status Solidi B* **172**, 539 (1992).
 - [3] R. P. Dias and I. F. Silvera, *Science* **355**, 715 (2017).
 - [4] N. W. Ashcroft, *Phys. Rev. Lett.* **21**, 1748 (1968).
 - [5] J. Boronat, C. Cazorla, D. Colognesi, and M. Zoppi, *Phys. Rev. B* **69**, 174302 (2004).
 - [6] G. Roma, C. M. Bertoni, and S. Baroni, *Solid State Commun.* **98**, 203 (1996).
 - [7] J. L. Martins, *Phys. Rev. B* **41**, 7883 (1990).
 - [8] S. J. Duclos, Y. K. Vohra, A. L. Ruoff, S. Filipek, and B. Baranowski, *Phys. Rev. B* **36**, 7664 (1987).
 - [9] R. Ahuja, O. Eriksson, and B. Johansson, *Phys. B (Amsterdam, Neth.)* **265**, 87 (1999).
 - [10] A. Lazicki, P. Loubeyre, F. Occelli, R. J. Hemley, and M. Mezouar, *Phys. Rev. B* **85**, 054103 (2012).
 - [11] Y. Wang, R. Ahuja, and B. Johansson, *Phys. Status Solidi B* **235**, 470 (2003).
 - [12] S. Lebègue, M. Alouani, B. Arnaud, and W. E. Pickett, *Europhys. Lett.* **63**, 562 (2003).
 - [13] W. Yu, C. Jin, and A. Kohlmeier, *J. Phys. Condens. Matter* **19**, 086209 (2007).
 - [14] A. Grüneis, *J. Chem. Phys.* **143**, 102817 (2015).
 - [15] A. M. Molodets, D. V. Shakhrai, and V. E. Fortov, *J. Exp. Theor. Phys.* **118**, 896 (2014).
 - [16] Y. M. Chen, X. R. Chen, Q. Wu, H. Y. Geng, X. Z. Yan, Y. X. Wang, and Z. W. Wang, *J. Phys. D* **49**, 355305 (2016).
 - [17] B. Monserrat, N. D. Drummond, and R. J. Needs, *Phys. Rev. B* **87**, 144302 (2013).
 - [18] H. Dammak, E. Antoshchenkova, M. Hayoun, and F. Finocchi, *J. Phys.: Condens. Matter* **24**, 435402 (2012).
 - [19] S. Baroni, S. D. Gironcoli, A. D. Corso, and P. Giannozzi, *Rev. Mod. Phys.* **73**, 515 (2001).
 - [20] I. Errea, M. Calandra, and F. Mauri, *Phys. Rev. B* **89**, 064302 (2014).
 - [21] P. Giannozzi *et al.*, *J. Phys.: Condens. Matter* **21**, 395502 (2009).
 - [22] P. E. Blöchl, *Phys. Rev. B* **50**, 17953 (1994).
 - [23] J. P. Perdew, K. Burke, and M. Ernzerhof, *Phys. Rev. Lett.* **77**, 3865 (1996).
 - [24] H. J. Monkhorst and J. D. Pack, *Phys. Rev. B* **13**, 5188 (1976).
 - [25] N. Marzari, D. Vanderbilt, A. De Vita, and M. C. Payne, *Phys. Rev. Lett.* **82**, 3296 (1999).
 - [26] M. Born and K. Huang, *Dynamical Theory of Crystal Lattices* (Clarendon, Oxford, 1954).
 - [27] I. Errea, M. Calandra, and F. Mauri, *Phys. Rev. Lett.* **111**, 177002 (2013).
 - [28] F. Birch, *Phys. Rev.* **71**, 809 (1947).
 - [29] Y. Kondo and K. Asaumi, *J. Phys. Soc. Jpn.* **57**, 367 (1988).
 - [30] J. Zhang, L. Zhang, T. Cui, Y. Li, Z. He, Y. Ma, and G. Zou, *Phys. Rev. B* **75**, 104115 (2007).
 - [31] G. Grimvall, B. Magyari-Köpe, V. Ozoliš, and K. A. Persson, *Rev. Mod. Phys.* **84**, 945 (2012).
 - [32] P. Souvatzis, O. Eriksson, M. I. Katsnelson, and S. P. Rudin, *Phys. Rev. Lett.* **100**, 095901 (2008).
 - [33] O. Hellman, I. A. Abrikosov, and S. I. Simak, *Phys. Rev. B* **84**, 180301 (2011).
 - [34] R. Bianco, I. Errea, L. Paulatto, M. Calandra, and F. Mauri, *Phys. Rev. B* **96**, 014111 (2017).